

Wetting critical behavior within the Lindblad dissipative dynamics

Claudia Artiano,^{1,*} Andrea Nava,^{2,3} and Michele Fabrizio⁴

¹*Department of Physics, KTH Royal Institute of Technology, Stockholm 106 91, Sweden*

²*Dipartimento di Fisica, Università della Calabria, Arcavacata di Rende I-87036, Cosenza, Italy*

³*INFN - Gruppo collegato di Cosenza, Arcavacata di Rende I-87036, Cosenza, Italy*

⁴*Scuola Internazionale Superiore di Studi Avanza (SISSA), via Bonomea 265, 34136, Trieste, Italy*

We investigate the critical behavior, both in space and time, of the wetting interface within the coexistence region around the first-order phase transition of a fully-connected quantum Ising model in a slab geometry. For that, we employ the Lindblad master equation in which temperature is inherited by the coupling to a dissipative bath rather than being a functional parameter as in the conventional Cahn's free energy. Lindblad's approach gives not only access to the dissipative dynamics and steady-state configuration of the wetting interface throughout the whole phase diagram but also shows that the wetting critical behavior can be successfully exploited to characterize the phase diagram as an alternative to the direct evaluation of the free energies of the competing phases.

I. INTRODUCTION

Wetting is generally defined as the ability of liquids to maintain contact with solid surfaces. More specifically, the study of wetting concerns the understanding of the relationship between bulk phase transitions and surfaces [1–9]. Clearly, this problem is extremely vast and rich. Wetting phenomena have been investigated in a variety of systems ranging from classical ones, such as in liquid-vapor phase transitions or binary liquid mixtures of linear alkanes and methanol, to polymeric mixtures, superfluid ^4He on thin cesium substrates, liquid ^3He on superfluid ^4He , dilute ultra-cold gases undergoing Bose-Einstein condensation, and many others [10–17].

In this study, we focus on the wetting layer that can form in the coexistence region accompanying a first-order phase transition [18]. Indeed, even though the wetting phenomenon has been extensively studied in the last forty years [19, 20], there are still open issues about quantum first-order phase transitions. Several attempts to disclose the wetting phenomenon in the quantum realm have relied on the quantum-classical mapping, i.e., on the idea that the properties of d -dimensional quantum systems at zero temperature and across a phase transition correspond to those of classical systems in higher dimensions [21]. Adopting a simple fully connected quantum spin Ising model, the authors of Ref. [18] observe that the critical properties of wetting in the quantum case indeed correspond to the classical ones in higher dimensions, specifically $d + 1$ in that simple mean-field model. However, the singular behavior of quantum fluctuations is different from that of classical fluctuations at finite temperature.

In this article, we perform a direct study of the dynamics and the equilibrium configuration of the wetting layer at phase coexistence in an open quantum system. We consider a slab geometry constituted by L layers, which is a discrete version of the model of Ref. [18]; each

layer is modeled by a quantum Ising model with N fully-connected sites. In the thermodynamic limit, $N \rightarrow \infty$, the mean-field approximation becomes exact, and the equilibrium state of the system can be found by solving a set of self-consistency equations. The same single-layer model already possesses a non-trivial phase diagram that, depending on the form of the spin-spin interactions, can display first- or second-order quantum and thermal phase transitions. Thanks to its simplicity, such a model has been widely employed in the past [22–24], for instance, to study the relaxation dynamics towards equilibrium in presence of dissipation [25, 26].

Specifically, we define the single-layer Hamiltonian such that it may undergo a first-order phase transition, and set its parameters so that the layer is in the coexistence region. Each layer is in turn coupled to its nearest neighbors as well as to a dissipative bath. We fix the boundary conditions of the whole slab imposing that the first and last layers are, respectively, in the ordered and disordered phases. In that way, we can easily study inhomogeneous phenomena, including wetting.

The presence of the dissipating baths coupled with each layer makes the system an open one. In open quantum systems, one is usually interested in describing the dynamics of a system (S) coupled to an external environment (E). In particular, one would like to derive a master equation for S, integrating out the degrees of freedom of E. In order to accomplish this task, we resort to the Lindblad master equation (LE) formalism. The LE is among the most popular master equations and has been employed in various and different contexts [27–33]. Starting from the microscopic Hamiltonian of the full system S+E, the LE can be derived within the weak S-E coupling approximation. That entails three further approximations: the Born, the Markov, and the rotating-wave approximation (see Ref. [27] for more details). Nonetheless, it can be shown that the LE is the most general time-local generator that preserves hermiticity, complete positivity, and unity of the trace of the system's density matrix, i.e., it is a so-called Krauss operator (see Ref. [34]). Here, we assume a Lindblad dynamics of each layer with jump operators defined through the instantaneous mean-field

* artiano@kth.se

Hamiltonian. This allows us to investigate arbitrarily large systems, and to explore the wetting phenomenon without resorting to Cahn's free energy functionals in which temperature enters just as a functional parameter [1], while in our case temperature is inherited by the bath. We show that, within our model and LE scheme, the wetting phenomenon spontaneously emerges during the quantum dissipative dynamics. That allows us to uncover in detail static and dynamic properties of the wetting interface as a function of the Hamiltonian parameters and the bath temperature.

The paper is organized as follows. In Section II we present the model Hamiltonian of a single-layer fully connected quantum Ising model and review its dissipative dynamics yielded by the Lindblad equation. In Section III we extend the formalism discussed in the previous Section to a multi-layer setup in which multiple copies of the single-layer system are connected one after the other to form a slab of length L . Each bulk layer is coupled to a dissipating bath while the states of the first and last layers are kept fixed. Section IV is devoted to the discussion of the relaxation and equilibrium properties of the multi-layer system. In particular, we analyze the behavior of the layer-resolved equilibrium energy, order parameter, and relaxation time. Finally, in Section V we summarize our results and discuss possible further perspectives of our work.

II. SINGLE-LAYER SYSTEM

In this Section, we briefly mention the properties of the single layer when it is decoupled from all the others. In particular, we discuss its phase diagram and show how to construct the Lindblad jump operators to describe its relaxation dynamics to the closest stationary state.

A. The quantum spin model for the single-layer system

We model each layer as a quantum Ising model on an N -site fully connected graph, described by the general Hamiltonian [22–24]

$$H = -h_x \sum_i \sigma_i^x - N \sum_{n=2}^m J_n \left(\frac{1}{N} \sum_i \sigma_i^z \right)^n \quad (1)$$

where $m \geq 2$ is an integer number, σ_i^α , with $\alpha = x, y, z$, are the Pauli matrices on site $i = 1, \dots, N$, h_x is the transverse magnetic field, and J_n are the n -spin exchange constants. In the following, we concentrate on the case $J_2 \neq 0$, $J_4 \neq 0$, and $J_{n \neq 2,4} = 0$, for which the model (1) undergoes a first-order phase transition [18, 35]: increasing either the temperature T or the transverse field h_x , the system goes from an ordered, ferromagnetic phase (F) to a disordered, paramagnetic one (P).

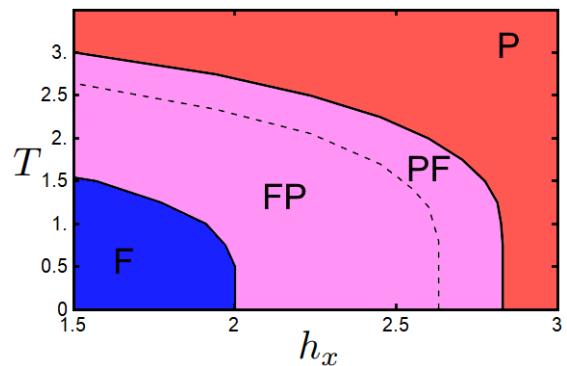


FIG. 1. Phase diagram of the single-layer model. In the region labeled as F, there is only a ferromagnetic free-energy minimum, and the Z_2 symmetry is broken. Conversely, in region P there is only a paramagnetic minimum. FP and PF denote the coexistence regions: in FP, the absolute minimum is ferromagnetic; in PF, it is paramagnetic. The F-P phase transition occurs along the dashed line separating FP from PF, and it takes place when the free energies cross. The solid lines between F and FP, and between P and PF, are spinodal lines where an additional metastable free energy minimum appears beside the stable one.

Thus, our single-layer system Hamiltonian reads

$$H = -h_x \sum_i \sigma_i^x - \frac{J_2}{N} \left(\sum_i \sigma_i^z \right)^2 - \frac{J_4}{N^3} \left(\sum_i \sigma_i^z \right)^4. \quad (2)$$

The phase diagram of the model (2) has been already studied in the past: it is illustrated in Fig. 1.

Thanks to the full connectivity of Hamiltonian (2), mean-field approximation becomes exact in the thermodynamic limit $N \rightarrow \infty$, as ensured by the vanishing of the covariance

$$\langle \sigma_i^\alpha \sigma_j^\beta \rangle - \langle \sigma_i^\alpha \rangle \langle \sigma_j^\beta \rangle \rightarrow \frac{1}{N} \xrightarrow{N \rightarrow \infty} 0. \quad (3)$$

It follows that the equilibrium Boltzmann distribution is given by

$$\rho \xrightarrow{N \rightarrow \infty} \prod_i \rho_i = \prod_i \frac{e^{-\beta H_i}}{\text{Tr}(e^{-\beta H_i})} \quad (4)$$

where ρ_i is a positive definite 4×4 matrix with unit trace, and the single site Hamiltonian H_i reads

$$H_i = -h_x \sigma_i^x - h_z(\mathbf{m}) \sigma_i^z, \quad (5)$$

with

$$h_z(\mathbf{m}) = 2J_2 m_z + 4J_4 m_z^3. \quad (6)$$

$\mathbf{m} = (m_x, m_y, m_z)$ indicates the Bloch vector, with components

$$m_\alpha := \frac{1}{N} \sum_i \langle \sigma_i^\alpha \rangle. \quad (7)$$

Notice that the Bloch vector verifies $|\mathbf{m}| \leq 1$, where the equality is fulfilled only by pure states, and that the single-site density matrix can be written as $\rho_i = \frac{1}{2}(1 + \mathbf{m} \cdot \boldsymbol{\sigma}_i)$. Thanks to the exact validity of the mean-field approximation, we can consider a single spin at a time and drop the index i .

It is easy to show that, when the system is at equilibrium with a bath at temperature T , its state is determined by a set of self-consistency equations:

$$\mathbf{m} = \tanh \beta h(\mathbf{m}) (\cos \theta(\mathbf{m}), 0, \sin \theta(\mathbf{m})) \quad (8)$$

where

$$\tan \theta(\mathbf{m}) = \frac{h_z(\mathbf{m})}{h_x}, \quad (9)$$

$$h(\mathbf{m}) = \sqrt{h_x^2 + h_z(\mathbf{m})^2}. \quad (10)$$

B. Lindblad master equation for the single layer

In the following, we describe the dissipative dynamics of open quantum systems in terms of LE formalism. Under the Born approximation the system-environment density matrix is factorized at any time, i.e.,

$$\rho_{S+E}(t) \simeq \rho_S(t) \otimes \rho_E(t), \quad \forall t. \quad (11)$$

Integrating out the environment degree of freedom under the Markov approximation one arrives at the following general form of the LE:

$$\begin{aligned} \dot{\rho}_S(t) = & -i [H_S, \rho_S(t)] \\ & + \sum_{\lambda} \left[\gamma_{\lambda} \left(2L_{\lambda} \rho_S(t) L_{\lambda}^{\dagger} - \{L_{\lambda}^{\dagger} L_{\lambda}, \rho_S(t)\} \right) \right. \\ & \left. + \bar{\gamma}_{\lambda} \left(2L_{\lambda}^{\dagger} \rho_S(t) L_{\lambda} - \{L_{\lambda} L_{\lambda}^{\dagger}, \rho_S(t)\} \right) \right], \quad (12) \end{aligned}$$

where H_S indicates the system Hamiltonian. The LE describes a dynamical map that is linear, completely positive, and trace preserving.

Neglecting pure dephasing processes, the dissipative dynamics of the system can be described by non-Hermitian jump operators that produce transitions between two eigenstates of the system Hamiltonian H_S :

$$L_{\lambda(m,n)} = |m\rangle\langle n|, \quad E_n < E_m. \quad (13)$$

It is easy to verify that the Boltzmann distribution is a stationary solution of Eq. (12) if $\gamma_{\lambda}/\bar{\gamma}_{\lambda} = e^{-\beta\epsilon_{\lambda}}$ with $\epsilon_{\lambda} = E_m - E_n > 0$. In the following, we set

$$\bar{\gamma}_{\lambda} = \Gamma f(-\beta\epsilon_{\lambda}/2) \quad (14)$$

with $f(x)$ the Fermi-Dirac distribution function, and Γ the overall bath-system coupling strength.

Ref. [25] extensively discusses many possible ways in which the Lindblad jump operators can be defined to

capture the physics of the simple model (2). Here, we consider one choice that, we will argue, allows correctly reproducing the dynamics of the wetting interface in the multi-layer system, see Sec. IV, and recovering the semiclassical results of Ref. [18].

Starting from a factorized density matrix, the full connectivity of the model (2) ensures that it remains factorized at any time:

$$\rho_S(t) \xrightarrow{N \rightarrow \infty} \prod_i \rho_i(t) \quad (15)$$

where $\rho_i(t)$ describes the time evolution of the spin i , coupled to a bath at temperature T and in the presence of a time-dependent magnetic field given by Eqs. (5)-(6):

$$\mathbf{h}(t) := \mathbf{h}(\mathbf{m}(t)) \quad (16)$$

$$:= \left(h_x, 0, 2J_2 m_z(t) + 4J_4 (m_z(t))^3 \right) \quad (17)$$

with

$$\mathbf{m}(t) = \frac{1}{N} \sum_i \text{Tr}(\rho_S(t) \boldsymbol{\sigma}_i), \quad (18)$$

which is self-consistently determined by the system's time evolution. Notice that the mean-field nature of the model is at the origin of the self-consistency of the dissipative dynamics. Hence, we can formally define a time-dependent system Hamiltonian as

$$H_t := -\mathbf{h}(t) \cdot \boldsymbol{\sigma} := -|\mathbf{h}(t)| \mathbf{v}_3(t) \cdot \boldsymbol{\sigma}, \quad (19)$$

which is just a two-level system Hamiltonian with time-dependent magnetic field. From Eq. (13), we can write the instantaneous Lindblad jump operators

$$\begin{aligned} L(t) = & |1\rangle\langle 0| = (\mathbf{v}_1(t) - i\mathbf{v}_2(t)) \cdot \boldsymbol{\sigma}/2 \\ & := \mathbf{v}^-(t) \cdot \boldsymbol{\sigma}/2, \quad (20) \end{aligned}$$

and its Hermitian conjugate

$$L^{\dagger}(t) = |0\rangle\langle 1| := \mathbf{v}^+(t) \cdot \boldsymbol{\sigma}/2, \quad (21)$$

where

$$\mathbf{v}^+(t) \wedge \mathbf{v}^-(t) = 2\mathbf{v}_3(t), \quad (22)$$

$$\mathbf{v}^+(t) = (\mathbf{v}^-(t))^*. \quad (23)$$

The energy difference between the eigenvalues of the instantaneous Hamiltonian is simply $\epsilon(t) = 2|\mathbf{h}(t)|$. Thus, $\bar{\gamma}(t)$ and $\gamma(t)$ depend on time.

In turn, this yields a LE with time-dependent parameters, where the expectation value of the spin operator is given by

$$\begin{aligned} \dot{\mathbf{m}}(t) = & \text{Tr}(\dot{\rho}_S(t) \boldsymbol{\sigma}) = -2\mathbf{h}(t) \wedge \mathbf{m}(t) \\ & - \frac{\gamma(t)}{2} \left[4(\mathbf{v}_3(t) + \mathbf{m}(t)) - \mathbf{v}^-(t)(\mathbf{v}^+(t) \cdot \mathbf{m}(t)) \right. \\ & \quad \left. - \mathbf{v}^+(\mathbf{v}^-(t) \cdot \mathbf{m}(t)) \right] \\ & + \frac{\bar{\gamma}(t)}{2} \left[4(\mathbf{v}_3(t) - \mathbf{m}(t)) + \mathbf{v}^-(t)(\mathbf{v}^+(t) \cdot \mathbf{m}(t)) \right. \\ & \quad \left. + \mathbf{v}^+(t)(\mathbf{v}^-(t) \cdot \mathbf{m}(t)) \right]. \quad (24) \end{aligned}$$

In Ref. [25], it has been shown that the Lindblad jump operators (20)–(21) are not able to capture the long time dynamics of the single-layer system, which remains trapped at all times in the closest stationary state, even if metastable. To describe the full dynamics, both at short and long times, and the relaxation to the true equilibrium state, one needs to write the master equation as a sum of competing terms, one for each phase (either stable or metastable). In this way, both supercooling and Mpemba effect emerge during the dissipative dynamics. Fortunately, we will not need such a complicated master equation to describe the relaxation and equilibrium dynamics of the wetting layer, as will become clear in the next Sections.

III. MULTI-LAYER SYSTEM

In this Section, we introduce the multi-layer model that we are going to investigate in the next Sections. We discuss how we introduce the inhomogeneities at the boundaries, and how we couple each layer in the bulk to a bath in order to study the relaxation and equilibrium dynamics of the wetting interface.

A. The quantum spin model for the multi-layer system

Let us now consider a multi-layer system composed of L layers, where each layer is modeled by the Hamiltonian in Eq. (2), and it is coupled to its nearest neighbor layers via quadratic and a quartic terms:

$$H_T = \sum_{\ell=1}^L H_{\ell} - \sum_{\ell=1}^{L-1} \left\{ \frac{\tilde{J}_2}{N} \left(\sum_{i \in \ell} \sigma_i^z \right) \left(\sum_{i \in \ell+1} \sigma_i^z \right) + \frac{\tilde{J}_4}{N^3} \left(\sum_{i \in \ell} \sigma_i^z \right)^2 \left(\sum_{i \in \ell+1} \sigma_i^z \right)^2 \right\}, \quad (25)$$

where H_{ℓ} is the Hamiltonian (2) for layer ℓ .

In the thermodynamic limit, the mean-field single site Hamiltonian for layer ℓ , dropping the site index, reads

$$H_{*\ell} = -h_x \sigma_{\ell}^x - \left(2\tilde{J}_2 m_{\ell}^z + 4\tilde{J}_4 m_{\ell}^{z3} \right) \sigma_{\ell}^z - \tilde{J}_2 \left(m_{\ell-1}^z + m_{\ell+1}^z \right) \sigma_{\ell}^z - 2\tilde{J}_4 \left(m_{\ell-1}^{z2} + m_{\ell+1}^{z2} \right) m_{\ell}^z \sigma_{\ell}^z. \quad (26)$$

In the following, we will set $\tilde{J}_n = J_n/2$; hence, when the multi-layer system is in the homogeneous case, i.e., all the layers are in the same state, Eq. (26) reduces to the single-layer Hamiltonian of Eq. (5).

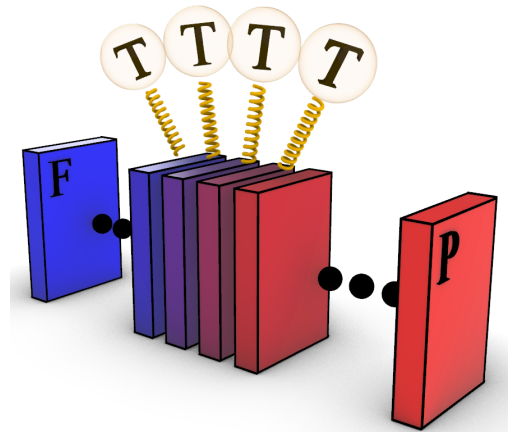


FIG. 2. Graphical representation of the model. We consider a multi-layer system composed of L layers. The first and the last layers are fixed: they are set to the ferromagnetic (F) and paramagnetic (P) state, respectively. All the other layers are coupled to a heat bath at temperature T , as schematized by the springs.

B. Lindblad master equation for the multi-layer system

We wish to study the dynamics of the wetting layer when the single layer is within the coexistence phase illustrated in Fig. 1. Within the coexistence phase, the single layer presents both stable and metastable phases. In the FP region, the ferromagnetic minima are stable (i.e., have a lower free-energy), and the paramagnetic is metastable; viceversa in the PF region. To model the presence of the wetting layer, we fix the first and the last layers of the multi-layer system in the ferromagnetic (F) and paramagnetic (P) phase, respectively. All the other layers are coupled to a heat bath and are free to evolve in time. The system is depicted in Fig. 2.

Following the same line of reasoning of Sec. II for the case of a single layer, we can write the dissipative dynamics of the full system considering a time-dependent magnetic field for each layer ℓ which is self-consistently determined by the system dynamics. From Eq. (26), the time-dependent magnetic field, accounting both for the intra- and inter-layer interactions is

$$\mathbf{h}_{\ell}(t) := \left| \mathbf{h}_{\ell}(\mathbf{m}_{\ell}(t), \mathbf{m}_{\ell-1}(t), \mathbf{m}_{\ell+1}(t)) \right| \mathbf{v}_{\ell}^3(\mathbf{m}_{\ell}(t), \mathbf{m}_{\ell-1}(t), \mathbf{m}_{\ell+1}(t)) \quad (27)$$

$$:= \left[h_x, 0, J_2 m_{\ell}^z(t) + 2J_4 m_{\ell}^{z3}(t) + J_2/2 (m_{\ell-1}^z(t) + m_{\ell+1}^z(t)) + J_4 (m_{\ell-1}^{z2}(t) + m_{\ell+1}^{z2}(t)) m_{\ell}^z(t) \right]. \quad (28)$$

From Eq. (27), we can define the single-layer time-dependent jump operators, similarly to Eqs. (20)–(21), the only difference being that both the magnitude and

the direction of the time-dependent magnetic field $\mathbf{h}_\ell(t)$ vary between layers. In fact, for each layer ℓ , we obtain a LE for the expectation value of the magnetization similar to Eq. (24), in which $\mathbf{h}(t)$, $\mathbf{v}_3(t)$, $\mathbf{v}^+(t)$, $\mathbf{v}^-(t)$ depend on $\mathbf{m}_\ell(t)$, $\mathbf{m}_{\ell-1}(t)$, $\mathbf{m}_{\ell+1}(t)$. Notice that the presence of the coupling between layers gives a set of coupled first-order non-linear differential equations that determine the wetting dynamics. Our implementation of the numerical solver for such a set of differential equations is provided at Ref. [36].

IV. RESULTS

In this Section, we discuss the results of the relaxation dynamics and equilibrium configuration of the multi-layer quantum spin model described in Sec. III, where inhomogeneities are introduced across the boundaries of the system in the presence of a first-order phase transition. Having set $\tilde{J}_n = J_n/2$ in the original Hamiltonian (25), the equilibrium phase diagram of the homogeneous multi-layer model reduces to the one of the single-layer case in Fig. 1 with the presence of a coexistence region where both the ferromagnetic, F, and paramagnetic, P, phases are minima of the free energy. In the following, we always set T and h_x within the coexistence region. In order to study interface phenomena, we consider a finite length L , multi-layer system, as depicted in Fig. 2, with the first and last layers, i.e., the boundaries, fixed in the F and P state respectively. At equilibrium, we expect that when T and h_x are in the FP (PF) phase, the bulk of the system lies in the F (P) phase while a small but finite region, i.e. the wetting region, forms near the last (first) layer of the slab. In the following, we discuss the energy cost and thickness of the wetting region as a function of the temperature and the magnetic field. Moreover, we discuss the dependence of the relaxation time on the bath coupling strength.

A. Energy

Let us start by looking at the relaxation dynamics in the $T \simeq 0.07$ (i.e., $T \approx 0$) limit, setting $J_n = 1$, in which case the coexistence region extends from $h_x \simeq 2$ to $h_x \simeq 2.83$ while the critical magnetic field that separates the FP and PF phases is $h_c \simeq 2.63113$. At $t < 0$, the system is prepared in its equilibrium minimum, i.e., all the layers are in the F (P) phase for h_x lower (higher) than h_c . The state of each layer is specified by the Bloch vector \mathbf{m}_F (\mathbf{m}_P) self-consistently determined by Eqs. (8)–(10). At $t = 0$ we fix the first and last layers into the F and P phase, respectively; at the same time, each layer in the bulk is connected with its own bath (see Fig. 2). Suddenly, the Bloch vector of each layer, \mathbf{m}_ℓ , starts to evolve in time while each layer exchanges energy with its neighbors and with the bath in order to reach the new equilibrium configuration that minimizes the energy

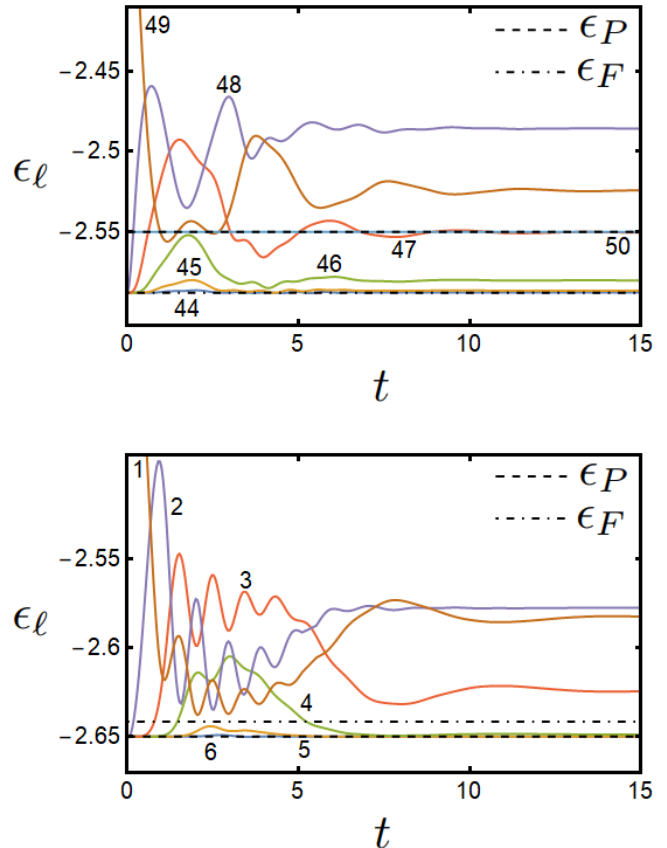


FIG. 3. Layer-resolved time evolution of the energy for a system of $L = 50$ layers for $\Gamma = 0.2$, in the FP phase ($h_x = 2.55$, top panel), and in the PF phase ($h_x = 2.65$, bottom panel). In both cases, the first layer is constrained into the F phase, the last layer into the P phase. The dot-dashed line is the energy of the homogeneous F phase (ϵ_F), the dashed line is the energy of the homogeneous P phase (ϵ_P). Only the layers closer to the corresponding metastable boundary are explicitly shown as the energy of the layers in the bulk overlaps with the energy of the stable minima, i.e. $\min[\epsilon_F, \epsilon_P]$. The label ℓ of each layer is shown near each curve. Color online.

of the multi-layer system, compatibly with the inhomogeneity introduced via the boundaries.

In Fig. 3 we plot the time evolution of the single-layer energy, defined as

$$\begin{aligned} \epsilon_\ell = & -h_x m_\ell^x - \frac{J_2}{2} m_\ell^{z^2} - \frac{J_4}{2} m_\ell^{z^4} \\ & - \frac{J_2}{4} (m_{\ell-1}^z + m_{\ell+1}^z) m_\ell^z \\ & - \frac{J_4}{4} ((m_{\ell-1}^z)^2 - (m_{\ell+1}^z)^2) m_\ell^{z^2}, \quad (29) \end{aligned}$$

obtained numerically by integrating the nonlinear LE given by Eqs. (24) and (27). We consider a bath coupling strength $\Gamma = 0.2$ and magnetic field along x below, $h_x = 2.55$ (top panel), and above, $h_x = 2.65$ (bot-

tom panel), the critical value h_c . From now on, we refer with ϵ_F (ϵ_P) to the single-layer energy of a homogeneous system with magnetization vector \mathbf{m}_F (\mathbf{m}_P), i.e., $\epsilon_F \equiv \epsilon_\ell(\mathbf{m}_\ell = \mathbf{m}_F \forall \ell)$ ($\epsilon_P \equiv \epsilon_\ell(\mathbf{m}_\ell = \mathbf{m}_P \forall \ell)$).

Notice that the single-layer energy has an intra-layer contribution plus an inter-layer term. At $t = 0$, when the inhomogeneities at the boundaries are created, all the layers deep in the bulk of the system have the same energy as in the stable homogeneous configuration. On the contrary, a large energy contribution emerges from the inter-layer term at the metastable boundary, due to the discontinuity in the magnetization between the boundary layer in the metastable phase ($\ell = L$ for the FP case and $\ell = 1$ for the PF one) and its neighboring layer (see the brown curve in both panels of Fig. 3). In the early stage of dynamics, in order to reduce the total energy, the order parameters of the layers around the metastable boundary start to rearrange assuming intermediate values between \mathbf{m}_F and \mathbf{m}_P in order to make the discontinuity smoother. Doing so, while the intra-layer energy contribution increases, the inter-layer energy of the boundary drastically decreases driving the system, at large t , into a new inhomogeneous equilibrium configuration with the formation of a wetting interface.

At equilibrium, moving along the wetting interface, from the metastable boundary towards the bulk, the single-layer energy ϵ_ℓ is a non-monotonous function of the distance from the boundary. Plotting the equilibrium values of ϵ_ℓ as a function of the magnetization m_ℓ^z (see Fig. 3), we observe that the energy increases and then decreases until it reaches the stable value $\min[\epsilon_F, \epsilon_P]$ inside the bulk as if it were virtually climbing up the (pseudo)potential barrier that separates the metastable and stable phases at the boundaries. This interpretation becomes clearer if we refer to the energy that each layer would have in the homogeneous case at fixed m_ℓ^z , which we plot in Fig. 4 (blue dots) together with the equilibrium energies (red dots) of the layers forming the wetting interface, same data of Fig. 3. We note that the blue dots strictly follow the energy landscape, climbing up the potential barrier that separates the metastable minima from the stable one, while the red dots describe a new energy landscape of the inhomogeneous system.

We emphasize that, with our choice of jump operators, albeit the single-layer would remain forever trapped in the metastable phase [25], the same unphysical metastability does not occur in the inhomogeneous slab. Indeed, we find that the profile of the wetting region is independent of the initial state and the bath-system coupling strength Γ . For instance, if we initialize the bulk layers in the metastable minimum, only the dissipation dynamics and the total relaxation time are affected but *not* the equilibrium configuration, which is always the stable one. The same happens if we start with an inhomogeneous configuration where P and F regions alternate. This guarantees that the approach we take yields physically sound results.

We also mention that, if we start in the FP phase and

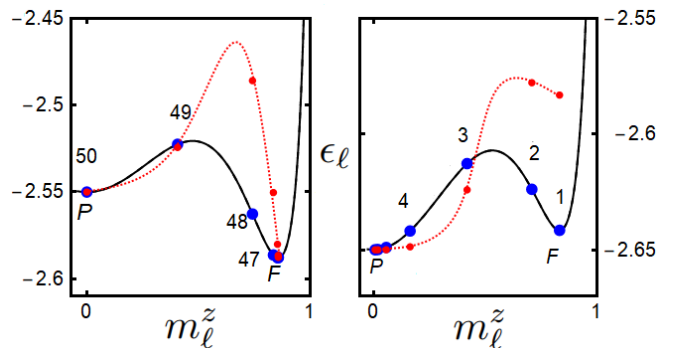


FIG. 4. Black line: energy per layer, ϵ_ℓ , of the homogeneous system as a function of the order parameter for $h_x = 2.55$ (FP, left panel) and $h_x = 2.66$ (PF, right panel). Blue dots: energy per layer in a homogeneous system at fixed magnetization m_ℓ^z . Red dots: equilibrium energy of the layers closer to the metastable boundary in the presence of the wetting interface (i.e., corresponding to the equilibrium values in Fig. 3). The red line is a guide for the eye, representing the (pseudo)potential for the inhomogeneous system.

initialize the bulk with domain walls between F^+ , i.e., $m_\ell^z > 0$, and F^- , i.e., $m_\ell^z < 0$, regions, interfaces emerge with m_ℓ^z switching from positive to negative passing through layers in the disordered phase m_ℓ^z . Such an interface has exactly the same shape as the wetting interface at the boundary between the P and F phase but is now doubled around the central P layer. Although these composite $F^\pm - P - F^\mp$ domain walls have an energy cost, they can move inside the system and annihilate with each other. This behavior is similar to the formation and propagation of solitons in trans-polyacetylene chains [37]. Studying the dynamics of domain walls between two equivalent stable minima in the coexistence region goes beyond the scope of this work and will be discussed in a forthcoming publication. This effect does not emerge in the PF phase where the $F^\pm - F^\mp$ domain walls are destroyed by the bath in favor of the stable ordered phase P.

B. Thickness

The wetting layer extent is expected to increase in size as the critical magnetic field, h_c , is approached. Indeed, as $h \rightarrow h_c$, one has $|\epsilon_F - \epsilon_P| \rightarrow 0$. It follows that, in order to smooth out the discontinuity, the system prefers to unpin more and more layers at the boundary from the stable phase towards the metastable one. In fact, the nearer we are to the critical magnetic field, the lower the intra-layer energy contribution is, while the inter-layer one becomes dominant.

In the PF phase ($h > h_c$), we define the amplitude of

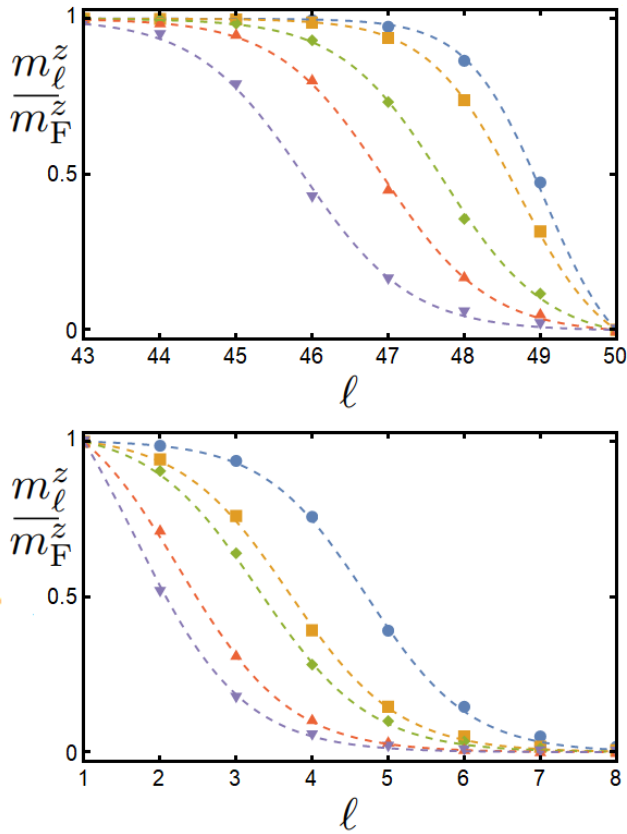


FIG. 5. Layer-resolved equilibrium value of the order parameter in the FP (top panel) and PF (bottom panel) phase for $\Gamma = 0.2$ and different values of the magnetic field along x , h_x . Only the eight nearest layers to the metastable boundary are shown. Top panel: $h_x = 2.55$ (blue circles), 2.6 (yellow squares), 2.628 (green diamonds), 2.6295 (red triangles), 2.631 (purple inverted triangles). Bottom panel: $h_x = 2.632$ (blue circles), 2.635 (yellow squares), 2.64 (green diamonds), 2.7 (red triangles), 2.8 (purple inverted triangles). The dashed lines correspond to the fit obtained through Eq.32.

the wetting interface due to the F phase as

$$\mathcal{A}_F = \sum_{\ell=1}^L \frac{m_\ell^z}{m_F^z}, \quad (30)$$

while in the FP phase ($h < h_c$) we define the wetting amplitude due the P phase as

$$\mathcal{A}_P = \sum_{\ell=1}^L \left(1 - \frac{m_\ell^z}{m_F^z} \right) = L - \mathcal{A}_F. \quad (31)$$

By looking at the wetting surface shown in Fig. 5, we observe that, even for $|h_c - h_x| \approx 10^{-4}$, only a small finite number of layers around the metastable boundary is involved, so that the equilibrium configuration is not affected by the system length L , i.e. $\mathcal{A}_{F/P} \ll L$. Clearly, in the case $\mathcal{A}_{F/P} \approx L$ the system length must be increased accordingly in order to avoid finite size effects. The data

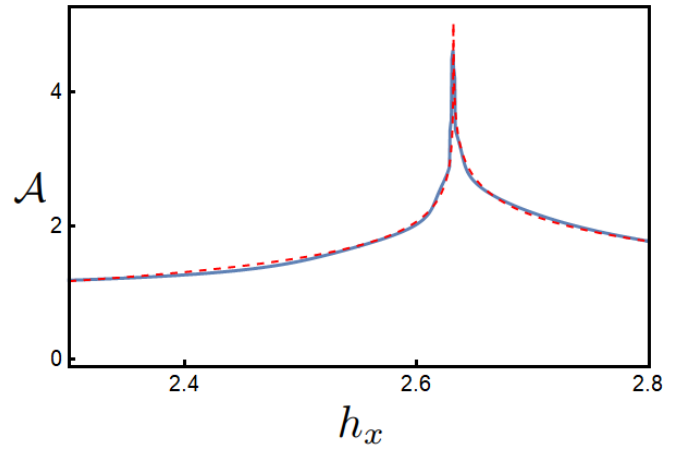


FIG. 6. Blue curve: wetting amplitude, $\mathcal{A} = \min[\mathcal{A}_F, \mathcal{A}_P]$, of the wetting region as a function of the transverse magnetic field, h_x , for $T = 0.2$ and $\Gamma = 0.2$. Red curve: logarithmic fit $f(h_x) := a - b \ln |h_x - h_c|$ with $a = 0.75$, $b = 0.38$ for $h_x < h_c$, and $a = 1$, $b = 0.43$ for $h_x > h_c$.

in Fig. 5 can be fitted by a two parameter function of the form

$$f(\alpha, \beta) = \frac{\tanh(\beta L - \alpha) - \tanh(\beta \ell - \alpha)}{\tanh(\beta L - \alpha) - \tanh(\beta - \alpha)}, \quad (32)$$

similar to the solitons bond-alternation domain walls in polyacetylene [37], or the non-equilibrium stationary state occupation number profile of an interacting fermionic chain [38]. This behavior is substantially different from the exponential decay expected for the second-order phase transitions [39].

In Fig. 6 we show the wetting amplitude \mathcal{A} as a function of the magnetic field h_x for a system at finite temperature $T = 0.2$. As discussed, the wetting interfaces increases approaching the critical magnetic field and diverges at $h_x = h_c$, where the phase transition between the FP and PF phases takes place. In agreement with the continuum limit discussed in Ref.18, we find that the wetting thickness diverges logarithmically as $\mathcal{A}_{F/P} = a_{F/P} - b_{F/P} \ln |h_x - h_c|$, similarly as in the classical case at the thermal phase transition [3].

The results of Fig. 6 can be extended at any temperature and any magnetic field within the coexistence region of the homogeneous system, see Fig. 1. In particular, the discussions above remain valid by reinterpreting our results in terms of free energy rather than energy at zero temperature [18]. In Fig. 7, we report the wetting amplitude for all the (T, h_x) values corresponding to the coexistence region of the single-layer phase diagram. Just by looking at the divergence of the wetting amplitude \mathcal{A} , we are able to recover FP-PF critical line, as can be observed by comparing Fig. 7 with the single-layer phase diagram in Fig. 1.

This result is nontrivial. In order to access the critical line that separates the two metastable phases in a first-order phase transition, standard approaches require

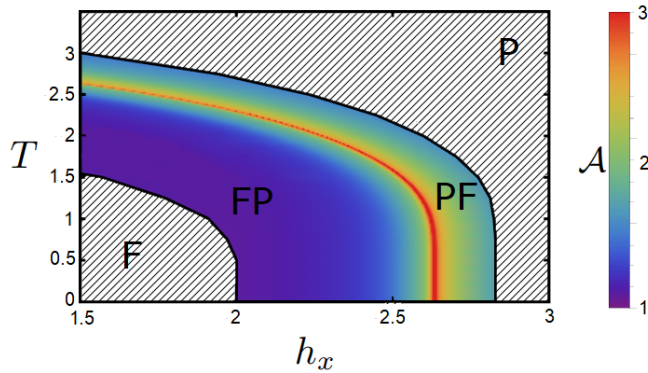


FIG. 7. $\mathcal{A} = \min[\mathcal{A}_F, \mathcal{A}_P]$ of the wetting layer as a function of the magnetic field and temperature, for $\Gamma = 0.2$.

solving self-consistent equations of the form of Eqs. (8)–(10) and then comparing all the free energy minima at a given value of the parameters (such as temperature and magnetic field). This requires computing, as soon as $T \neq 0$, the entropy of the system, which is often a cumbersome task. In addition, standard LE approaches are only able to recover the F-FP and PF-P critical lines, while failing to recover the FP-PF transition line within the coexistence region [25]. On the contrary, in the multi-layer setup discussed in this paper, thanks to the inhomogeneities introduced by the boundary conditions, it is possible to implement the standard self-consistent LE approach to the full phase diagram. Within the LE approach, the only required ingredients are the instantaneous Hamiltonian eigenvectors that define the Lindblad jump operators, see Eq. (24), at the given bath temperature, see Eq. (14). It follows that the full phase diagram at any finite T can be easily derived.

Before moving on to the next Section, let us compare the results obtained within the LE approach for the multi-layer system with the results obtained within the semiclassical analysis on a continuum semi-infinite slab, see Eq. (35) in Ref. [18]. In Fig. 8, we plot, for different values of h_x , m_ℓ^z/m_F^z as a function of the layer index ℓ , obtained within the LE approach (dots), together with the same quantity computed within the continuum limit formula [18] (dashed lines). We observe a remarkable quantitative agreement between the results of the two approaches as long as h_x is not too close to h_c . As $h_x \rightarrow h_c$, the wetting interface of the discrete model is thicker than the continuum one (the leftmost in the top panel, the rightmost in the bottom panel). Such disagreement simply derives from the fact that the interface width is controlled in the continuum limit by the stiffness term, second-order expansion in the interlayer distance of the coupling among layers, and that can well change quantitatively the results, but not the critical behavior.

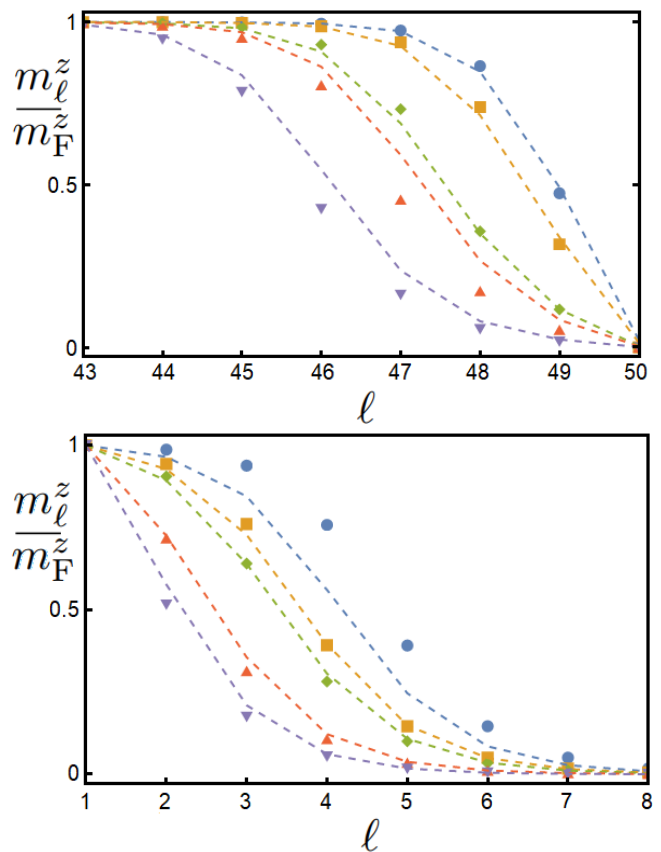


FIG. 8. Layer-resolved equilibrium value of the order parameter, normalized to the corresponding m_F^z , in the FP (top panel) and PF (bottom panel) phase, for $\Gamma = 0.2$ and different values of the transverse magnetic field, h_x . The markers represent the discrete model, the dashed lines the continuum limit within the semiclassical approximation (see main text). Only the eight nearest layers to the metastable boundary are shown. Top panel: $h_x = 2.55$ (blue circles), 2.6 (yellow squares), 2.628 (green diamonds), 2.6295 (red triangles), 2.631 (purple inverted triangles). Bottom panel: $h_x = 2.632$ (blue circles), 2.635 (yellow squares), 2.64 (green diamonds), 2.7 (red triangles), 2.8 (purple inverted triangles).

C. Time

In this Section, we discuss the relaxation time, τ , defined as the time required to reach equilibrium, as a function of the magnetic field, h_x , and the bath coupling strength, Γ . In Fig. 9 we show τ as a function of h_x at $T = 0.2$ and three different values of the bath strength. Far from h_c , the relaxation time is independent of h_x and reaches a steady value that, as intuitively expected, decreases for increasing bath strength Γ , i.e., a stronger bath dissipates faster. Furthermore, for each value of Γ we observe a critical slowing down: the relaxation time has a power-law divergence approaching h_c , $\tau \sim |h_x - h_c|^{-\alpha}$, with the critical exponent that is function of the bath coupling strength, $\alpha(\Gamma)$. We find $\alpha(0.2) = 1.4$, $\alpha(0.5) = 1.8$, and $\alpha(0.9) = 2.1$, respec-

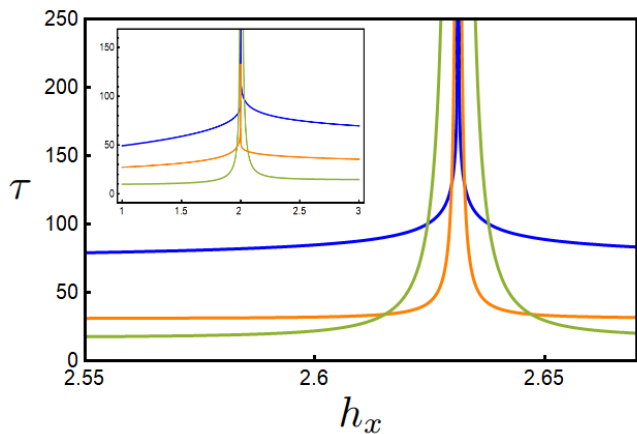


FIG. 9. Relaxation time to reach the equilibrium configuration for a system initialized in the F phase, if $h < h_c$, and P phase, if $h > h_c$, as a function of h_x , for $T = 0.2$, and $\Gamma = 0.1$ (blue/upper), 0.2 (yellow/middle) and 0.5 (green/lower). The first layer is constrained into the F phase and the last layer into the P phase. Inset: relaxation time for a second order phase transition, where the critical magnetic field is $h_c = 2$. Color online.

tively.

As a consequence, relaxation time curves for different Γ intersect with each other for some value of the magnetic field h_x . It follows that for each value of h_x we can define an optimal dissipation through the finite value of Γ that maximizes the system-bath energy exchange rate. This dissipative optimal working point, represented by a minimum of $\tau(\Gamma)$ as shown in Fig. 10 for four different values of the magnetic field, is similar to the non-equilibrium optimal working point that emerges in the non-equilibrium stationary state of systems coupled with two baths [38, 40, 41]. Indeed, when a system is coupled to two different baths that induce a particle/energy flow, one observes a change in the monotonicity of the non-equilibrium stationary current as a function of the applied bias, which represents the optimal performance of the bath. The existence of an optimal working point is a consequence of the presence, in dissipative dynamics, of two timescales: an intrinsic timescale induced by the Hamiltonian of the system, and a dissipative timescale set by the bath strength Γ . As long as the former is shorter than the latter, increasing Γ increases the performance of the bath, i.e., reduces τ . When the two timescales are comparable, the system and the bath are in resonance and the energy transfer is maximum. Finally, when the bath becomes too strong, the natural evolution induced by the Hamiltonian and the dissipative one induced by the bath through the jump operators (that are themselves a function of the Hamiltonian) are desynchronized, and they slow each other down. Consequently, the relaxation times increase with Γ . Finally, we observe that moving towards the critical line the optimal working point moves to lower values of the coupling Γ . It is also worth noting that, albeit in our discussion we made use of values of

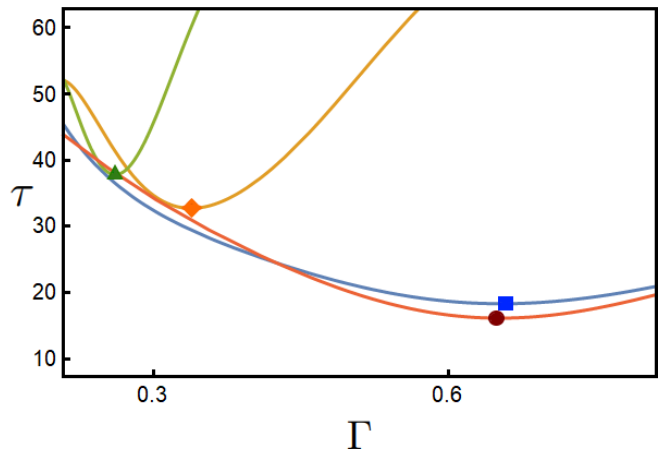


FIG. 10. Relaxation time to reach the equilibrium configuration for a system initialized in the F phase, if $h < h_c$, and P phase, if $h > h_c$, as a function of Γ for $T = 0.2$ and different values of the magnetic field in proximity of h_c . The marks represent the optimal working points (minima of the curve) for $h_x = 2.60$ (blue square), 2.62 (yellow rhombus), 2.62 (green triangle) and 2.66 (red circle). The first layer is constrained into the F phase and the last layer into the P phase.

the coupling Γ of the order of 10^{-1} , for better plot rendering, the same behavior is observed for lower values of the coupling, i.e., the ultra-weak regime, where the LE is, in general, more physically sound.

We verified the existence of an optimal working point also in a single-layer system with second-order phase transition like the one described by Eq. (1) for $J_n = 0$, $\forall n \neq 2$ (see also Ref. [25]) as shown in the inset of Fig. 9. In such a way, we support the idea that the presence of the optimal working point is not a consequence of the inhomogeneities induced by the fixed boundary condition but, rather, an intrinsic property of the self-consistent dissipative dynamics.

The results shown in Fig. 9 can be extended to the full phase diagrams as done for the wetting amplitude \mathcal{A} suggesting that also the relaxation time can be used to extract, numerically or experimentally, the critical line in the coexistence region.

V. CONCLUSIONS

We have discussed the main static and dynamic features of the wetting interface that emerges in the coexistence region of a first-order transition, both quantum and thermal, when at the surface the metastable phase is favored over the stable one present in the interior of the bulk. For that, we have considered a prototype mean-field model that displays a first-order phase transition both at zero and finite temperatures, a fully-connected quantum Ising model with two and four spin exchange in a slab geometry. Instead of using a time-dependent Cahn's free-energy functional, as often done,

we have simulated the dynamics through the Lindblad master equation, where the temperature is directly inherited by the coupling to a dissipative bath. In this way, we are able to study the wetting phenomenon at any temperature and Hamiltonian parameters. In particular, we reproduce the known critical behavior of the wetting interface length as the first-order transition is approached [3]; we also identify a critical behavior of the relaxation time, with bath-dependent exponents, which reveals the emergence in the parameter space of a dissipative optimal working point where the relaxation time is minimum.

Moreover, our analysis suggests a way to characterize the phase diagram alternative to the direct comparison between the free energies of the coexisting phases, which exploits the critical behavior in space and time of the wetting interface upon approaching the phase transition.

The reliability of the approach in recovering physically sound results, combined with its simplicity and versatility, could make it a precious tool to investigate both equilibrium and non-equilibrium phase transitions in open quantum systems paving the way to search for novel phases or phase transitions arising in spin models [42, 43] or junctions of interacting fermionic systems [44–50].

ACKNOWLEDGEMENTS

This work received funding from the European Research Council (ERC) under the European Union’s Horizon 2020 research and innovation program, Grant agreements No. 101001902 (C. A.) and No. 692670 (M. F.). A. N. acknowledges financial support from Italy’s MIUR PRIN projects TOP-SPIN (Grant No. PRIN 20177SL7HC).

-
- [1] J. W. Cahn, Critical point wetting, *J. Chem. Phys.* **66**, 3667 (1977).
- [2] C. Ebner and W. Saam, New phase-transition phenomena in thin argon films, *Phys. Rev. Lett.* **38**, 1486 (1977).
- [3] R. Lipowsky, Critical surface phenomena at first-order bulk transitions, *Phys. Rev. Lett.* **49**, 1575 (1982).
- [4] P.-G. De Gennes, Wetting: statics and dynamics, *Rev. Mod. Phys.* **57**, 827 (1985).
- [5] D. S. Fisher and D. A. Huse, Wetting transitions: A functional renormalization-group approach, *Phys. Rev. B* **32**, 247 (1985).
- [6] S. Dietrich, Wetting phenomena, in *Phase transitions and critical phenomena*, edited by C. Domb and J. L. Lebowitz (Academic Press, 1988) pp. 1–218.
- [7] S. Dietrich, Critical phenomena at interfaces, *Physica A* **168**, 160 (1990).
- [8] J. O. Indekeu, Introduction to wetting phenomena, *Acta Phys. Pol. B* **26**, 1065 (1995).
- [9] M. M. Telo da Gama, Theory of wetting and surface critical phenomena, in *Computer Simulations of Surfaces and Interfaces*, edited by B. Dünweg, D. P. Landau, and A. I. Milchev (Springer, 2003) pp. 239–258.
- [10] E. Cheng, M. W. Cole, W. Saam, and J. Treiner, Helium prewetting and nonwetting on weak-binding substrates, *Phys. Rev. Lett.* **67**, 1007 (1991).
- [11] P. Nacher and J. Dupont-Roc, Experimental evidence for nonwetting with superfluid helium, *Phys. Rev. Lett.* **67**, 2966 (1991).
- [12] J. Rutledge and P. Taborek, Prewetting phase diagram of ^4He on cesium, *Phys. Rev. Lett.* **69**, 937 (1992).
- [13] E. Cheng, M. Cole, J. Dupont-Roc, W. Saam, and J. Treiner, Novel wetting behavior in quantum films, *Rev. Mod. Phys.* **65**, 557 (1993).
- [14] P. Taborek and J. E. Rutledge, Tuning the wetting transition: Prewetting and superfluidity of ^4He on thin cesium substrates, *Phys. Rev. Lett.* **71**, 263 (1993).
- [15] H. Kellay, D. Bonn, and J. Meunier, Prewetting in a binary liquid mixture, *Phys. Rev. Lett.* **71**, 2607 (1993).
- [16] H. Alles, J. P. Ruutu, A. V. Babkin, and P. J. Hakonen, Wetting of superfluid ^4He by liquid ^3He , *Phys. Rev. Lett.* **73**, 1388 (1994).
- [17] J. Indekeu, Wetting phase transitions and critical phenomena in condensed matter, *Physica A* **389**, 4332 (2010), Proceedings of the 12th International Summer School on Fundamental Problems in Statistical Physics.
- [18] L. Del Re, M. Fabrizio, and E. Tosatti, Nonequilibrium and nonhomogeneous phenomena around a first-order quantum phase transition, *Phys. Rev. B* **93**, 125131 (2016).
- [19] D. Bonn, J. Eggers, J. Indekeu, J. Meunier, and E. Rolley, Wetting and spreading, *Rev. Mod. Phys.* **81**, 739 (2009).
- [20] W. D. Kaplan, D. Chatain, P. Wynblatt, and W. C. Carter, A review of wetting versus adsorption, complexions, and related phenomena: the rosetta stone of wetting, *J. Mater. Sci.* **48**, 5681 (2013).
- [21] J. A. Hertz, Quantum critical phenomena, in *Basic Notions of Condensed Matter Physics* (CRC Press, 2018) pp. 525–544.
- [22] C. Wang, Z. Qin, and D. Lin, First-order phase transition in order-disorder ferroelectrics, *Phys. Rev. B* **40**, 680 (1989).
- [23] B. Sciolla and G. Biroli, Dynamical transitions and quantum quenches in mean-field models, *J. Stat. Mech.* **2011**, P11003 (2011).
- [24] V. Bapst and G. Semerjian, On quantum mean-field models and their quantum annealing, *J. Stat. Mech.* **2012**, P06007 (2012).
- [25] A. Nava and M. Fabrizio, Lindblad dissipative dynamics in the presence of phase coexistence, *Phys. Rev. B* **100**, 125102 (2019).
- [26] A. Nava and M. Fabrizio, Dissipative cooling induced by pulse perturbations, *SciPost Phys.* **12**, 14 (2022).
- [27] H.-P. Breuer and F. Petruccione, *The Theory of Open Quantum Systems* (Oxford University Press, Oxford, 2007) p. 656.
- [28] T. Prosen, Open XXZ spin chain: Nonequilibrium steady state and a strict bound on ballistic transport, *Phys. Rev. Lett.* **106**, 217206 (2011).
- [29] B. Olmos, I. Lesanovsky, and J. P. Garrahan, Facilitated spin models of dissipative quantum glasses, *Phys. Rev.*

- Lett. **109**, 020403 (2012).
- [30] T. A. Brun, Continuous measurements, quantum trajectories, and decoherent histories, *Phys. Rev. A* **61**, 042107 (2000).
- [31] B. Kraus, H. P. Büchler, S. Diehl, A. Kantian, A. Micheli, and P. Zoller, Preparation of entangled states by quantum markov processes, *Phys. Rev. A* **78**, 042307 (2008).
- [32] D. Manzano, A short introduction to the Lindblad master equation, *AIP Adv.* **10**, 025106 (2020).
- [33] C. Artiago, F. Balducci, and A. Scardicchio, Signatures of many-body localization in the dynamics of two-level systems in glasses, *Phys. Rev. B* **103**, 214205 (2021).
- [34] M. M. Wilde, *Quantum Information Theory* (Cambridge University Press, 2013).
- [35] B. H. Teng and H. K. Sy, Phase diagrams of the transverse ising model with a four-spin interaction, *Europhys. Lett.* **73**, 601 (2006).
- [36] Our implementation of the numerical solver for the multi-layer system, <https://github.com/cartiaco/Wetting-with-Lindblad>.
- [37] A. J. Heeger, S. Kivelson, J. R. Schrieffer, and W. P. Su, Solitons in conducting polymers, *Rev. Mod. Phys.* **60**, 781 (1988).
- [38] A. Nava, M. Rossi, and D. Giuliano, Lindblad equation approach to the determination of the optimal working point in nonequilibrium stationary states of an interacting electronic one-dimensional system: Application to the spinless Hubbard chain in the clean and in the weakly disordered limit, *Phys. Rev. B* **103**, 115139 (2021).
- [39] G. Borghi, M. Fabrizio, and E. Tosatti, Surface dead layer for quasiparticles near a mott transition, *Phys. Rev. Lett.* **102**, 066806 (2009).
- [40] G. Benenti, G. Casati, T. Prosen, and D. Rossini, Negative differential conductivity in far-from-equilibrium quantum spin chains, *Europhys. Lett.* **85**, 37001 (2009).
- [41] G. Benenti, G. Casati, T. Prosen, D. Rossini, and M. Žnidarič, Charge and spin transport in strongly correlated one-dimensional quantum systems driven far from equilibrium, *Phys. Rev. B* **80**, 035110 (2009).
- [42] A. M. Tsvelik, Majorana fermion realization of a two-channel kondo effect in a junction of three quantum ising chains, *Phys. Rev. Lett.* **110**, 147202 (2013).
- [43] D. Giuliano, A. Nava, and P. Sodano, Tunable kondo screening length at a Y-junction of three inhomogeneous spin chains, *Nucl. Phys. B* **960**, 115192 (2020).
- [44] M. Oshikawa, C. Chamon, and I. Affleck, Junctions of three quantum wires, *J. Stat. Mech.* **2006**, P02008 (2006).
- [45] C.-Y. Hou and C. Chamon, Junctions of three quantum wires for spin- $\frac{1}{2}$ electrons, *Phys. Rev. B* **77**, 155422 (2008).
- [46] D. Giuliano, L. Lepori, and A. Nava, Tunable spin/charge kondo effect at a double superconducting island connected to two spinless quantum wires, *Phys. Rev. B* **101**, 195140 (2020).
- [47] D. Giuliano and A. Nava, Dual fermionic variables and renormalization group approach to junctions of strongly interacting quantum wires, *Phys. Rev. B* **92**, 125138 (2015).
- [48] F. Buccheri, A. Nava, R. Egger, P. Sodano, and D. Giuliano, Violation of the Wiedemann-Franz law in the topological kondo model, *Phys. Rev. B* **105**, L081403 (2022).
- [49] D. Giuliano, A. Nava, R. Egger, P. Sodano, and F. Buccheri, Multiparticle scattering and breakdown of the Wiedemann-Franz law at a junction of n interacting quantum wires, *Phys. Rev. B* **105**, 035419 (2022).
- [50] D. Guerzi and A. Nava, Probing majorana zero modes by measuring transport through an interacting magnetic impurity, *Physica E* **134**, 114895 (2021).